Cancer Management and Research

Elevate Series

Open Access Full Text Article

ORIGINAL RESEARCH

Integrating Machine Learning Algorithms to Construct a Triaptosis-Related Prognostic Model in Melanoma

Jiaheng Xie[1,*], Min Zhang[1,*], Min Qi[2]

[1]Department of Plastic Surgery, Xiangya Hospital, Central South University, Changsha, 410008, People's Republic of China; [2]Department of Burns and Plastic Surgery, Shenzhen Hospital of Southern Medical University, Shenzhen, Guangdong, People's Republic of China

*These authors contributed equally to this work

Correspondence: Min Qi, Department of Burns and Plastic Surgery, Shenzhen Hospital of Southern Medical University, Shenzhen, Guangdong, People's Republic of China, Email qimin05@csu.edu.cn

Introduction: Melanoma is a highly aggressive skin cancer that accounts for a disproportionate number of skin cancer-related deaths due to early metastasis and therapy resistance. Programmed cell death (PCD), including ferroptosis and apoptosis, plays a crucial role in tumor progression and therapy response. Among these, triaptosis is a newly described form of PCD. It represents a novel mechanism of cell death with potential implications for cancer treatment. However, its role in melanoma remains largely unexplored.

Methods: We explored the role of triaptosis in melanoma by integrating single-cell and bulk RNA sequencing data. Key triaptosis-related genes and pathways were identified and incorporated into machine learning models to construct a prognostic signature. The TCGA-SKCM cohort served as the training dataset, and GEO datasets were used for validation.

Results: A robust prognostic model based on triaptosis-associated signature (TAS) was established using the SurvivalSVM algorithm. This model showed superior predictive performance, with consistently high concordance index (C-index) values across independent validation datasets. Kaplan–Meier survival analysis indicated that high-risk patients had significantly worse overall survival than low-risk patients. The model's predictive accuracy was confirmed through receiver operating characteristic (ROC) curve analysis and principal component analysis (PCA). Moreover, immune infiltration and tumor microenvironment (TME) analyses revealed significant associations between TAS and immune cell populations.

Conclusion: Triaptosis-related gene expression patterns are closely linked with melanoma prognosis and immune infiltration. Our findings provide novel insights into triaptosis as a potential biomarker and therapeutic target, offering strategies to overcome treatment resistance in melanoma.

Keywords: melanoma, cancer, tumor microenvironment, cell death, target

Introduction

Melanoma is the skin cancer originating from melanocytes, the pigment-producing cells predominantly located in the skin.[1–3] Accounting for less than 5% of all skin cancers, melanoma is responsible for the majority of skin cancer-related deaths due to its propensity for early metastasis and therapeutic resistance.[4–6] The incidence of melanoma has been steadily rising globally, particularly in populations with high levels of ultraviolet (UV) radiation exposure.[7,8] UV-induced DNA damage, genetic predisposition, and mutations in key genes such as BRAF, NRAS, and TERT are major contributors to melanoma pathogenesis.[9]

Recent advances in genomic profiling have enabled the identification of major driver mutations in melanoma, leading to the development of targeted therapies. BRAF mutations, particularly V600E, are the most common, and BRAF inhibitors (eg, vemurafenib, dabrafenib) combined with MEK inhibitors (eg, trametinib, cobimetinib) have shown significant survival benefits. For patients with NRAS mutations, MEK inhibitors have demonstrated limited efficacy, and ongoing trials are evaluating combination strategies. TERT promoter mutations, associated with increased telomerase

Received: 4 March 2025
Accepted: 28 May 2025
Published: 13 June 2025

activity and poor prognosis, currently lack direct targeted therapies but are being actively investigated as potential therapeutic targets.[10,11]

However, the overall prognosis for patients with advanced or metastatic melanoma remains poor, with five-year survival rates hovering around 30% for stage IV disease.[12] Resistance to both targeted therapies and immunotherapies remains a significant clinical challenge, necessitating the development of novel strategies for early diagnosis, risk stratification, and therapeutic targeting.[13] A deeper understanding of the molecular mechanisms driving melanoma progression and immune evasion is critical for addressing these unmet clinical needs.

Programmed cell death (PCD) is a fundamental biological process that maintains cellular homeostasis and eliminates damaged or abnormal cells.[14] In cancer, dysregulation of PCD mechanisms, including resistance to apoptosis and ferroptosis, enables tumor survival, immune evasion, and therapeutic resistance.[15] Apoptosis has been extensively studied in melanoma, with therapies such as BRAF inhibitors often inducing apoptotic pathways.[16] Ferroptosis, a recently discovered form of iron-dependent cell death, has also shown therapeutic promise in melanoma.[17] Despite these advances, there is a growing need to explore less-studied PCD pathways that may contribute to tumor progression and resistance mechanisms.

Triaptosis is a newly identified form of oxidative cell death, characterized by the accumulation of deidentified, phosphatidylinositol 3-phosphate (PI(3)P)-negative endosomes, followed by membrane blebbing and rupture.[18] Unlike traditional forms of programmed cell death, triaptosis is triggered by oxidative stress—specifically through agents like menadione sodium bisulfite (MSB), a pro-oxidant vitamin K precursor.[18] This mechanism involves the direct oxidation and inactivation of the PI(3)P-producing enzyme VPS34, leading to disruption of endosomal membrane dynamics and ultimately, cancer cell death. While triaptosis has been functionally validated in prostate cancer models, where MSB treatment yielded durable anti-tumor responses, its role in other malignancies remains largely unknown. Exploring the presence and regulatory mechanisms of triaptosis in melanoma could provide novel insights into tumor biology and uncover promising therapeutic strategies to overcome resistance to current treatments.[18] Investigating triaptosis in melanoma may uncover novel therapeutic targets and pathways to overcome resistance to current treatments. Constructing a prognostic model based on triaptosis-related signatures offers an opportunity to elucidate the role of this novel PCD pathway in melanoma. Such a model can identify critical genes and pathways associated with triaptosis, which may serve as biomarkers for risk stratification or targets for therapeutic intervention. By leveraging machine learning and integrating single-cell and bulk RNA-sequencing data, a robust triaptosis-related model could provide insights into the interplay between triaptosis, the tumor microenvironment, and immune regulation. Furthermore, accurate prognostic models are essential for guiding personalized treatment decisions and improving patient outcomes, particularly in a highly heterogeneous disease like melanoma.

In this study, we investigated the role of triaptosis in melanoma using a combination of single-cell and bulk RNA-sequencing datasets. We constructed a triaptosis-related prognostic model using machine learning techniques and validated its performance across multiple independent cohorts. Our findings not only highlight the clinical relevance of triaptosis in melanoma but also underscore its potential as a therapeutic target and biomarker in precision oncology.

Methods

Single-Cell RNA Dataset and Processing

The single-cell RNA-sequencing dataset (GSE215120) was obtained from the Gene Expression Omnibus (GEO).[19] The dataset underwent quality control using Seurat (v4.0) to exclude cells with low unique molecular identifier (UMI) counts, high mitochondrial gene content, or low gene complexity. Filtered cells were normalized and scaled, and highly variable genes were identified for downstream analysis. Principal component analysis (PCA) was performed to reduce the dimensionality of the data, and significant principal components (PCs) were selected based on an elbow plot and variance contributions. Uniform manifold approximation and projection (UMAP) was used for visualization of cell clusters. The clusters were annotated based on canonical marker genes and biological knowledge. The proportions of each cell type across samples were calculated and visualized as stacked bar plots.

The AUCell R package was used to calculate the enrichment scores of Triaptosis related genes in different cell types. The set of genes used isSupplemental Table 1. This gene set was obtained in a previously published study.[18]

All cells were divided into high and low groups based on a median score. Cell-cell communication was analyzed using the CellChat package. Interaction networks between cell types were inferred by evaluating ligand-receptor interactions based on known signaling pathways. The strength and number of interactions were quantified and compared between groups. Interaction networks were visualized with chord diagrams, and outgoing interaction strengths were plotted for each cell type.

Bulk RNA Sequencing Data Download and Analysis

Bulk RNA-sequencing data for melanoma patients from TCGA-SKCM and GEO datasets (GSE19234, GSE22153, GSE53118, GSE54467, GSE59455, GSE65904) were obtained using the TCGAbiolinks and GEOquery R packages, respectively.[20–25] TCGA data in FPKM format were converted to TPM, while GEO microarray data underwent background correction and normalization using limma. To correct for batch effects, the combined expression matrix was processed using the ComBat algorithm from the sva R package, with batch information (eg, "TCGA" or "GEO") specified to adjust for dataset-specific differences while preserving biological variability. Post-correction, PCA was used to confirm effective removal of batch effects, enabling downstream analyses such as differential expression and survival analysis with harmonized expression data.

Machine Learning Model Construction for Prognostic Prediction

We used the differentially expressed genes between the high and low TAS_ groups in single cell sequencing, as well as the related genes obtained by correlation analysis to construct the prognostic model. Using TCGA-SKCM as the training cohort and six GEO datasets (GSE19234, GSE22153, GSE53118, GSE54467, GSE59455, and GSE65904) as validation cohorts, we constructed prognostic model. Gene expression data were preprocessed by retaining shared genes across datasets, log-transforming, and z-score normalizing the expression matrices to ensure comparability. Batch effects were mitigated by cohort-specific scaling. A total of 101 machine learning algorithms and their combinations, including CoxBoost, Lasso, Random Survival Forest (RSF), plsRcox, and SurvivalSVM, were employed to construct prognostic models. Feature selection was performed in a pretraining step to identify the most predictive variables, with a minimum threshold of three features enforced for model stability. Final model performance was evaluated using concordance index (C-index) values across all independent validation cohorts, ranking models based on their average C-index. Risk scores for individual samples were calculated using the linear predictor method, and the best-performing models, along with their selected features, were saved for further analysis. C-index heatmaps were generated to visualize and compare the performance of all models and combinations across the cohorts, providing a comprehensive evaluation of prognostic capabilities.

Comparison of the Prognostic Value of the Triaptosis-Related Signature (TAS) with Published Melanoma Prognostic Models

To compare the prognostic value of the TAS model with currently published prognostic models related to cutaneous melanoma, we conducted a literature search in the PubMed database using keywords such as "melanoma", "features", and "prognostic model". The specific approach has been reported in our previous article.[26]

Using the triaptosis-related signature (TAS) features and genetic features extracted from all previously published prognostic models, we calculated the concordance index (C-index) values for each model in the TCGA cohort. These C-index values were then ranked in descending order, with the model achieving the highest C-index placed at the top. This approach facilitated a systematic comparison of the TAS model's prognostic performance against existing melanoma prognostic models.

Validation of the Optimal TAS Model Using Survival Analysis, ROC Curves, and PCA

To evaluate the predictive performance of the optimal triaptosis-related signature (TAS) model, we conducted survival analysis, receiver operating characteristic (ROC) curve analysis, and principal component analysis (PCA) on both the training cohort (TCGA-SKCM) and six independent validation datasets (GSE19234, GSE22153, GSE53118, GSE54467, GSE59455, and GSE65904).

Patients were divided into high-risk and low-risk groups based on the median risk score calculated using the TAS model. Kaplan-Meier survival curves were generated for each group, and differences in overall survival (OS) between the groups were evaluated using the Log rank test. Survival curves were plotted separately for the training and validation cohorts to assess the model's robustness across datasets.

The time-dependent ROC curves were plotted to evaluate the TAS model's predictive accuracy for overall survival at 1-, 3-, and 5-year time points. The area under the curve (AUC) was calculated for each time point using the timeROC R package. Higher AUC values indicate better predictive performance. The ROC curves were generated for both the training and validation cohorts, and the AUC values were compared across datasets to confirm the model's generalizability.

PCA was performed to assess the distribution of high-risk and low-risk patients in a dimensionality-reduced space. The expression profiles of the TAS-related genes were used as input for PCA. The first two principal components were visualized in scatter plots, showing the separation between the high-risk and low-risk groups in the training and validation cohorts. Clear separation between the two groups demonstrates the discriminative ability of the TAS model.

Immune Infiltration Analysis

The immune infiltration landscape was evaluated using the CIBERSORT algorithm, leveraging normalized RNA-seq data to estimate the proportions of 22 immune cell types based on the signature matrix. Samples were divided into high-risk and low-risk groups according to their risk scores. The differences in immune cell infiltration between these groups were assessed using statistical analysis. Heatmaps were generated to illustrate the distribution of immune cell infiltration across samples, with a color gradient reflecting the relative abundance of each immune cell type.

Tumor Microenvironment (TME) Analysis

The tumor microenvironment was characterized by calculating immune, stromal, and ESTIMATE scores using the ESTIMATE algorithm. The correlation between risk scores and these TME scores was evaluated using Spearman correlation analysis. The relationship between the scores and risk was visualized through scatter plots, with linear regression curves included to highlight trends. This analysis provided a detailed understanding of the interplay between the risk scores and the components of the tumor microenvironment.

GSEA Pathway Analysis

Pathway activity was analyzed using Gene Set Enrichment Analysis (GSEA) to evaluate enrichment scores for GO (Gene Ontology) and KEGG (Kyoto Encyclopedia of Genes and Genomes) pathways. Gene sets were curated from the MsigDB database, and GSEA was applied to generate enrichment scores for each pathway across all samples. Pathways significantly associated with high- and low-risk groups were identified and visualized using heatmaps, with a focus on pathways showing statistically significant differences.

Cell Culture and Transfection

The SK-MEL-48 cell line was purchased from ATCC and was cultured in DMEM supplemented with 10% fetal bovine serum (FBS) and 1% penicillin-streptomycin under standard conditions of 37°C with 5% CO_2. Cells were transfected with either si-control or si-LAPTM4B constructs using Lipofectamine 3000 (Invitrogen) according to the manufacturer's protocol.

Transwell Migration and Invasion Assay

To assess cell migration, transwell chambers (8 μm pore size; Corning) were used. For the migration assay, 2×10^4 cells in serum-free DMEM were seeded in the upper chamber, while the lower chamber was filled with DMEM containing 10% FBS as a chemoattractant. For the invasion assay, the upper chambers were pre-coated with Matrigel (BD Biosciences) before seeding 4×10^4 cells. After 24 hours of incubation, cells on the upper surface of the membrane were removed with a cotton swab, while cells that had migrated or invaded to the lower surface were fixed with 4% paraformaldehyde, stained with crystal violet, and counted under a microscope in five randomly selected fields.

Wound Healing Assay

The wound healing assay was performed to evaluate the effects of LAPTM4B knockdown on cell migration. Cells were seeded in 6-well plates and grown to confluence. A sterile pipette tip was used to create a straight scratch in the cell monolayer, and the debris was washed away with phosphate-buffered saline (PBS). Cells were then cultured in serum-free DMEM, and images of the wound area were captured at 0 and 24 hours using an inverted microscope. The wound closure rate was calculated as the percentage reduction in the wound area over time using ImageJ software.

Statistical Analysis

All statistical analyses were performed using R (v3.4.2; The R Foundation for Statistical Computing, Vienna, Austria). Descriptive statistics were used to summarize data, including means, medians, and standard deviations for continuous variables and proportions for categorical variables. Group comparisons were conducted using *t*-tests or Wilcoxon rank-sum tests for continuous data and chi-square tests for categorical data. Correlation analyses were performed using Spearman correlation coefficients. Survival analysis was conducted using Kaplan-Meier curves and the Log rank test to evaluate differences in overall survival. Cox proportional hazards regression models were applied to assess the association between variables and survival outcomes, with hazard ratios (HRs) and 95% confidence intervals (CIs) reported. Statistical significance was defined as a two-tailed p-value < 0.050. Data visualization, including heatmaps, scatter plots, and survival curves, was performed using ggplot2 and other R packages. All analyses ensured reproducibility through clearly documented scripts and methods.

Results

Cellular Heterogeneity and Triaptosis-Related Activity

Figure 1 illustrates the cellular heterogeneity and triaptosis-related activity across the analyzed dataset. UMAP analysis identified 14 distinct cell clusters (Figure 1A), which were annotated into six major cell types: epithelial, NKT, endothelial, fibroblasts, myeloid, and cycling cells (Figure 1B). Epithelial cells were the predominant population, as shown in their distribution across samples (Figure 1C). Marker gene analysis confirmed the identities of these cell types, with representative genes used for annotation displayed in Figure 1D.

Triaptosis-related activity, quantified by TAS scoring, demonstrated significant heterogeneity across cell populations. Notably, epithelial cells exhibited the highest TAS scores, indicating a potential role in triaptosis-associated mechanisms within the tumor microenvironment (Figure 1E and G). Cell-cell communication analysis revealed that the TAS-high group displayed markedly stronger intercellular interactions compared to the TAS-low group, with epithelial cells acting as central hubs in the TAS-high interaction network (Figure 1H–J). Correlation analysis (Figure 1K) identified the top 150 genes positively associated with TAS scoring, providing further insights into the molecular basis of triaptosis activity.

Performance of Prognostic Models Using SurvivalSVM

From the 101 machine learning algorithms screened, SurvivalSVM was identified as the best-performing model for prognostic prediction. Using TCGA-SKCM as the training cohort and six independent validation cohorts (GSE19234, GSE22153, GSE53118, GSE54467, GSE59455, GSE65904) for evaluation, SurvivalSVM achieved the highest concordance index (C-index) in the training cohort (Figure 2). Validation results across the six cohorts demonstrated

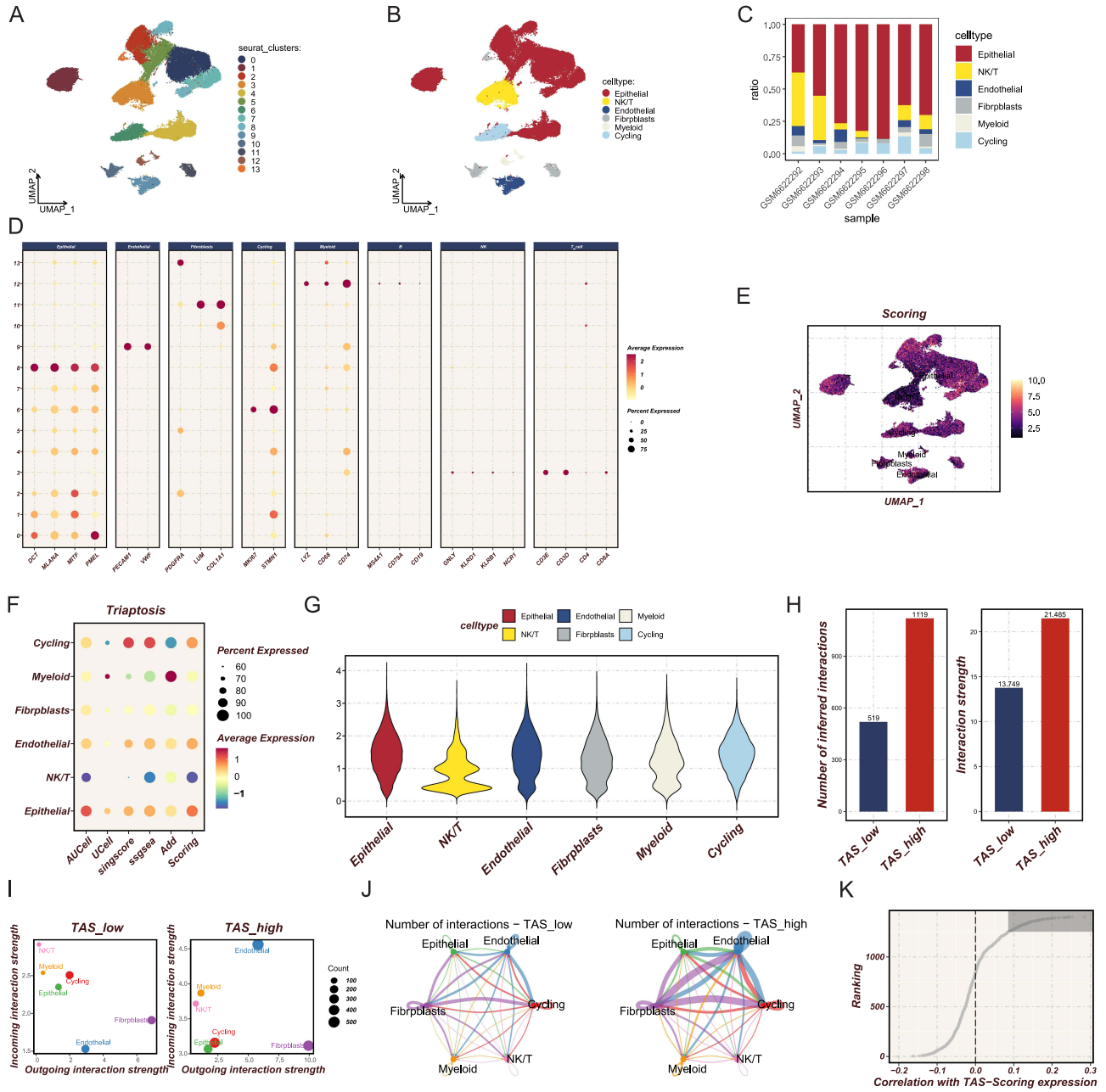

Figure 1 Cellular Heterogeneity and Triaptosis-Related Activity. (**A**) UMAP analysis identifies 14 distinct cell clusters across the dataset. (**B**) These clusters are annotated into six major cell types: epithelial, NKT, endothelial, fibroblasts, myeloid, and cycling cells. (**C**) The distribution of epithelial cells across different samples, showing their predominance. (**D**) Marker gene analysis confirming the identity of each cell type, with representative genes displayed. (**E, F**) Tas scores across cell populations, highlighting significant heterogeneity in triaptosis-related activity. (**G**) Epithelial cells exhibit the highest TAS scores, indicating their potential involvement in triaptosis within the tumor microenvironment. (**H–J**) Cell-cell communication analysis showing stronger intercellular interactions in the TAS-high group, with epithelial cells acting as central hubs in the interaction network. (**K**) Correlation analysis identifying the top 150 genes positively associated with TAS scores, providing insights into the molecular basis of triaptosis activity.

consistent and robust predictive performance, confirming the model's generalizability (Figure 2). The results underscore the strength of SurvivalSVM as an optimal prognostic model identified through comprehensive screening. Heatmaps visually summarize the C-index values across all cohorts, highlighting its superior performance compared to other algorithms. These findings establish SurvivalSVM as a reliable and effective tool for prognostic prediction in melanoma.

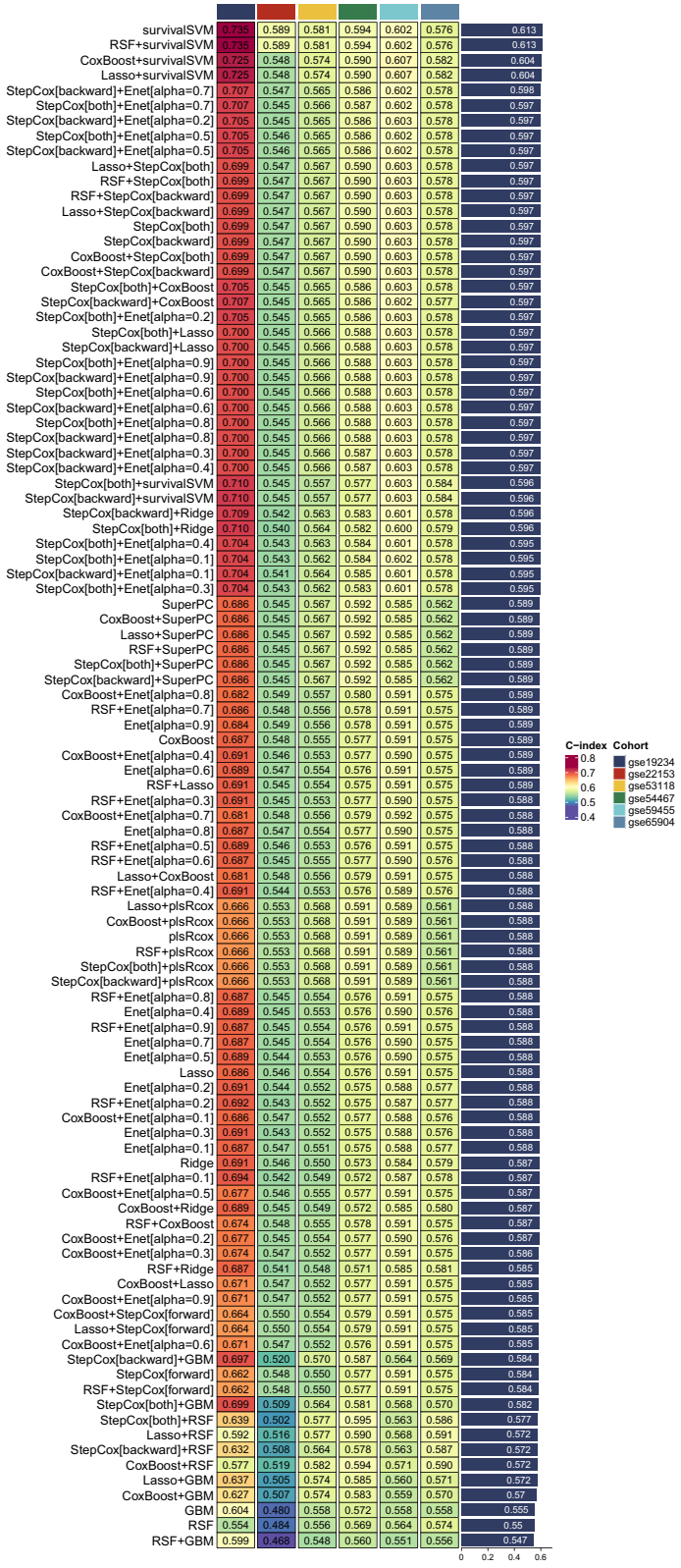

Figure 2 Performance of Prognostic Models Using SurvivalSVM. Performance of the SurvivalSVM model in the TCGA-SKCM training cohort and six independent validation cohorts (GSE19234, GSE22153, GSE53118, GSE54467, GSE59455, GSE65904). The model achieved the highest C-index in the training cohort and demonstrated robust predictive performance across the validation cohorts. Heatmaps summarize the C-index values, highlighting SurvivalSVM's superior performance compared to other machine learning algorithms.

https://doi.org/10.2147/CMAR.S525738

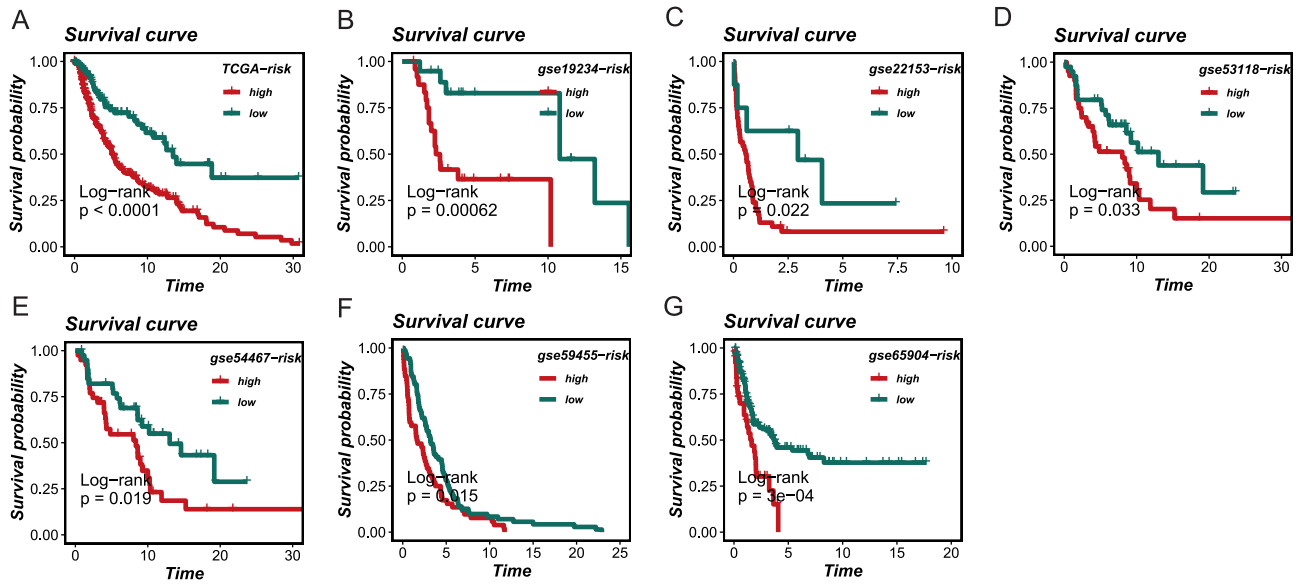

Figure 3 Survival Analysis of Risk Groups. Kaplan-Meier survival curves showing the prognostic stratification of the SurvivalSVM model in the TCGA training cohort (**A**) and validation cohorts (**B**–**G**). Patients in the high-risk group exhibited significantly worse overall survival compared to the low-risk group in all cohorts, confirming the model's effectiveness in stratifying risk groups and predicting survival outcomes.

Survival Analysis of Risk Groups

Kaplan-Meier survival analysis was conducted to evaluate the prognostic stratification ability of the SurvivalSVM model across the training and validation cohorts (Figure 3). In the TCGA training cohort, patients in the high-risk group exhibited significantly worse overall survival compared to the low-risk group (log-rank $p < 0.0001$; Figure 3A). Consistent results were observed across all six validation cohorts, including GSE19234 (log-rank $p < 0.001$; Figure 3B), GSE22153 (log-rank $p = 0.022$; Figure 3C), GSE53118 (log-rank $p = 0.033$; Figure 3D), GSE54467 (log-rank $p = 0.019$; Figure 3E), GSE59455 (log-rank $p = 0.015$; Figure 3F), and GSE65904 (log-rank $p<0.001$; Figure 3G). These results demonstrate that the SurvivalSVM-based prognostic model effectively stratifies patients into high- and low-risk groups with distinct survival outcomes, validating its robustness and utility for prognostic prediction.

Comparison of Prognostic Models with Published Bioinformatics Models

The performance of the SurvivalSVM prognostic model was compared to all bioinformatics models published in PubMed across both the training cohort (TCGA-SKCM) and six validation cohorts (GSE19234, GSE22153, GSE53118, GSE54467, GSE59455, GSE65904) (Figure 4A–G). The SurvivalSVM model achieved the highest C-index in the TCGA training cohort as well as in the GSE19234 and GSE59455 validation cohorts. These results highlight the model's superior predictive performance in these datasets. While it did not consistently achieve the highest C-index across all cohorts, the SurvivalSVM model remained highly competitive and consistently ranked among the top-performing models in all validation cohorts, demonstrating its robustness and generalizability.

ROC Curve and PCA Analysis

The predictive performance of the SurvivalSVM model was further evaluated using time-dependent ROC curves and PCA analysis. Time-dependent ROC curves (Figure 4H–N) highlighted the model's ability to predict survival outcomes at 1-, 3-, and 5-year interval. Across the six validation cohorts, the AUC values demonstrated consistent and reliable performance, supporting the model's applicability in external datasets.

PCA analysis (Figure 4O–U) showed distinct clustering of high- and low-risk groups in both the training and validation cohorts. The separation between risk groups reflected differences in molecular profiles, confirming the

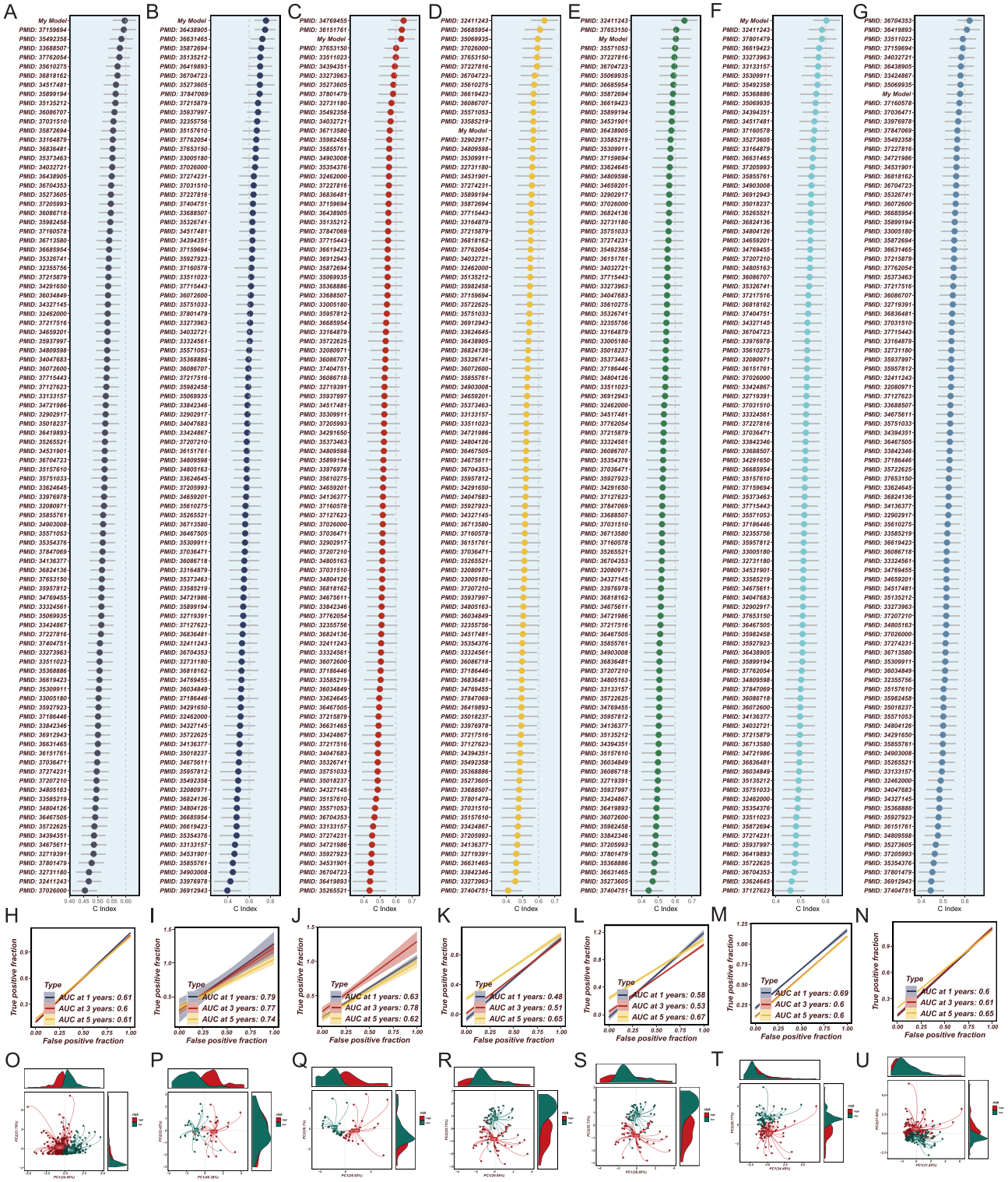

Figure 4 Comparison of Prognostic Models with Published Bioinformatics Models. (**A**–**G**) Comparison of the SurvivalSVM model with published bioinformatics models across the TCGA-SKCM training cohort and six validation cohorts. SurvivalSVM achieved the highest C-index in the TCGA-SKCM cohort and several validation cohorts, demonstrating its superior performance and robustness. (**H**–**N**) Time-dependent ROC curves assessing the model's predictive ability at 1-, 3-, and 5-year intervals across the validation cohorts. AUC values consistently support the model's reliable predictive performance. (**O**–**U**) PCA analysis showing distinct clustering of high- and low-risk groups, further validating the discriminative power of the SurvivalSVM model in both training and validation cohorts.

https://doi.org/10.2147/CMAR.S525738

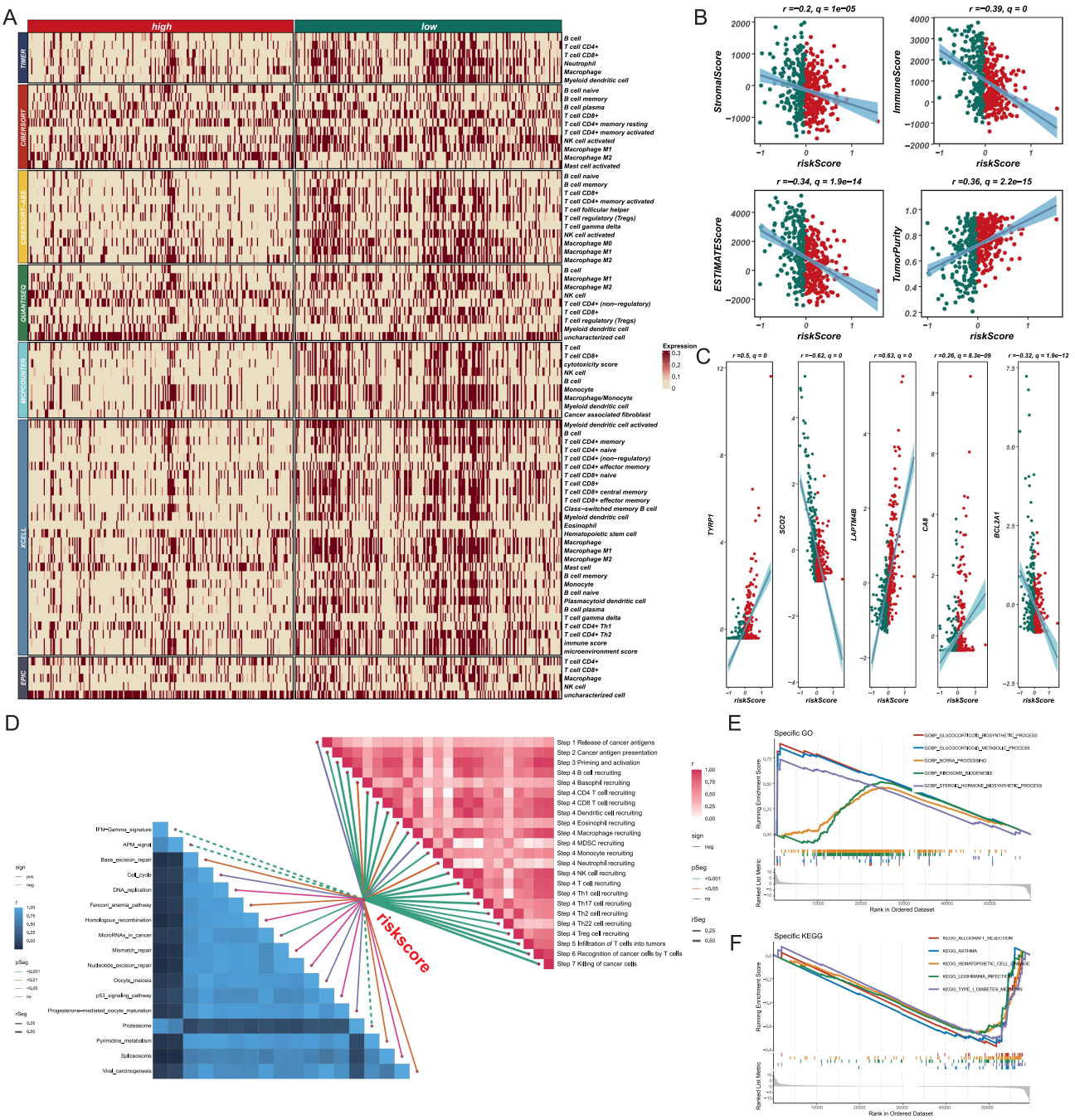

Figure 5 Immune and Tumor Microenvironment Analysis. (**A**) Heatmap of immune cell proportions between high- and low-risk groups, revealing reduced immune infiltration in high-risk samples. (**B**) Correlation analysis showing negative correlations between risk scores and immune/stromal/ESTIMATE scores, indicating immune suppression in high-risk samples. (**C**) Gene expression analysis of key model-associated genes (TYRP1, LAPTM4B, CA8, SCO2, BCL2A1), illustrating their correlation with risk scores. (**D**) GSVA pathway enrichment analysis showing associations between high-risk samples and immune suppression/tumor progression pathways. (**E** and **F**) GSEA results confirming the enrichment of immune-related pathways in the low-risk group, highlighting functional differences between risk groups.

discriminative power of the SurvivalSVM model. While the model's C-index varied across cohorts, its stratification of risk groups and predictive accuracy reinforce its clinical relevance.

Immune and Tumor Microenvironment Analysis

Figure 5 provides insights into immune infiltration and the tumor microenvironment (TME) in the context of the SurvivalSVM model. Heatmap analysis (Figure 5A) revealed significant differences in immune cell proportions between

high- and low-risk groups, with high-risk samples showing an overall reduction in immune infiltration. Correlation analysis (Figure 5B) demonstrated that risk scores negatively correlated with immune and stromal scores, as well as ESTIMATE scores, indicating a diminished immune presence in the high-risk group.

Key genes identified from the SurvivalSVM model included TYRP1, LAPTM4B, and CA8, which were positively correlated with the model, while SCO2 and BCL2A1 were negatively correlated with the model (Figure 5C). These findings highlight their potential roles in survival prediction and immune escape mechanisms. These findings highlight their potential roles in survival prediction and immune escape mechanisms. Furthermore, pathway enrichment analysis using GSVA (Figure 5D) indicated that high-risk samples were associated with pathways related to immune suppression and tumor progression. GSEA results (Figure 5E and F) further confirmed the enrichment of immune-related processes and pathways in the low-risk group, highlighting the functional differences between risk groups.

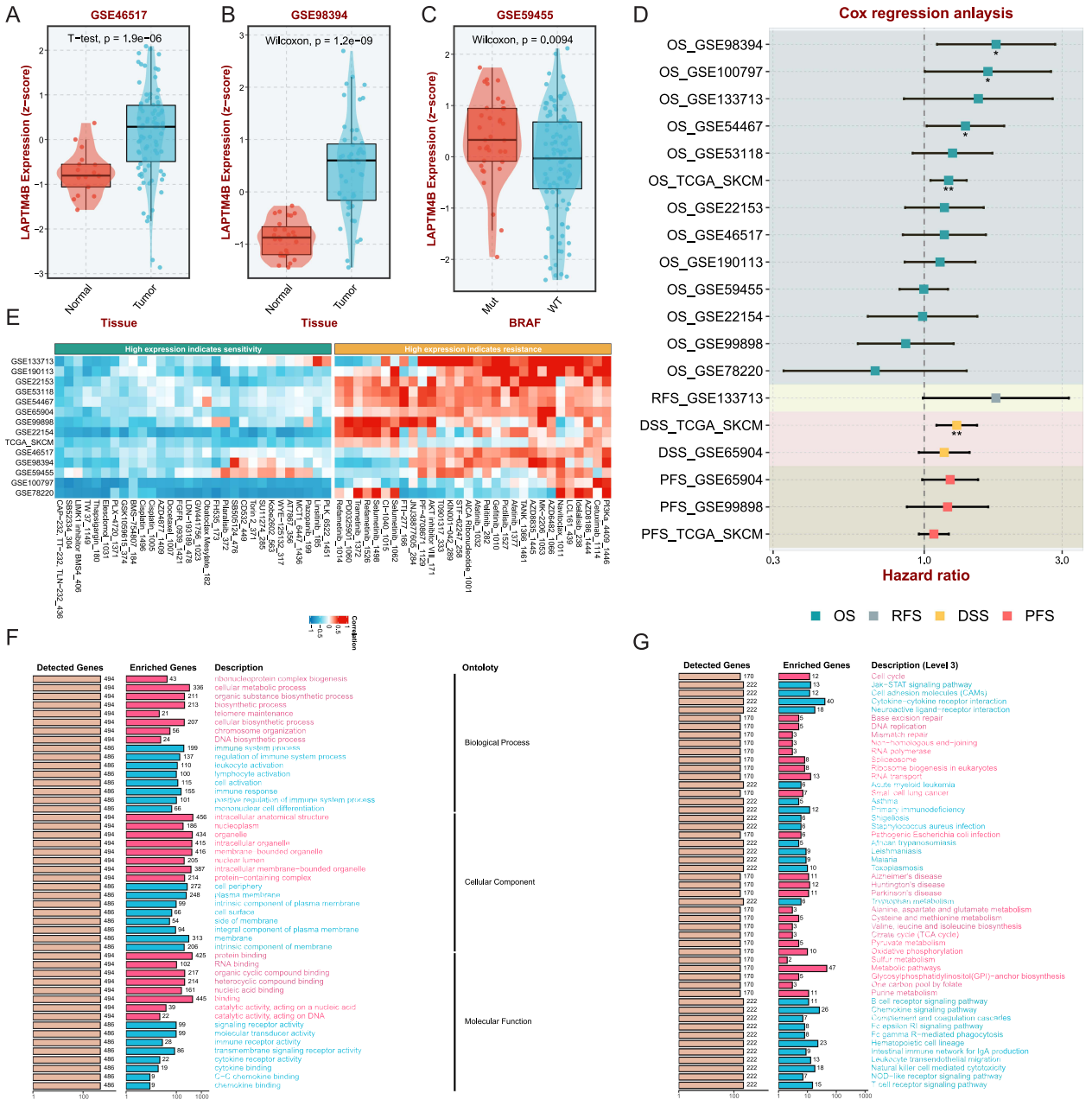

Figure 6 Continued.

https://doi.org/10.2147/CMAR.S525738

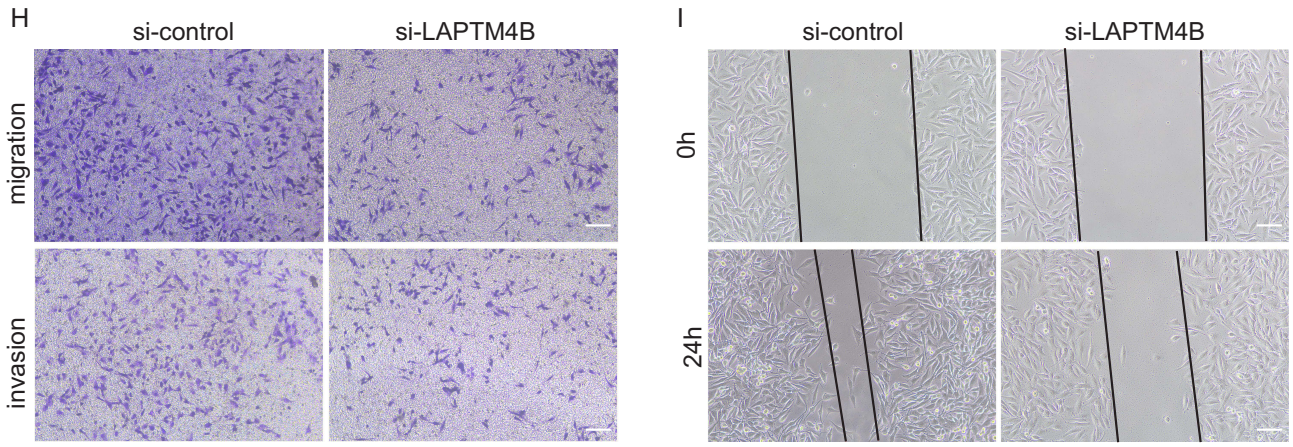

Figure 6 Functional Validation of LAPTM4B as a Key Model-Associated Gene. (**A**–**C**) Expression analysis of LAPTM4B in tumor versus normal tissues, showing significantly higher expression in tumors. Stratification by BRAF mutation status reveals differential expression. (**D**) Cox regression analysis indicating that higher LAPTM4B expression correlates with poorer survival outcomes, including OS, DSS, RFS, and PFS. (**E**–**G**) Functional enrichment analysis of LAPTM4B-associated genes, highlighting pathways related to cell migration, invasion, and immune suppression. (**H** and **I**) Experimental validation of LAPTM4B's role in tumor aggressiveness through functional assays. Knockdown of LAPTM4B (si-LAPTM4B) in SK-MEL-48 cells significantly reduced cell migration and invasion (**H**) and impaired wound healing (**I**), confirming LAPTM4B's role in promoting cellular migration and tumor progression.

Functional Validation of LAPTM4B as a Key Model-Associated Gene

The role of LAPTM4B, identified as the most positively correlated gene in the SurvivalSVM model, was experimentally validated (Figure 6). Analysis of multiple datasets demonstrated significantly higher LAPTM4B expression in tumor tissues compared to normal tissues (Figure 6A–C). Further stratification by BRAF mutation status revealed differential LAPTM4B expression, highlighting its potential relevance in specific genetic contexts.

Cox regression analysis across multiple datasets indicated that higher LAPTM4B expression was consistently associated with poorer overall survival (OS), disease-specific survival (DSS), relapse-free survival (RFS), and progression-free survival (PFS) (Figure 6D). Functional enrichment analysis of LAPTM4B-associated genes revealed involvement in pathways related to cell migration, invasion, and immune regulation. Notably, in Figure 6E and G, blue-shaded terms indicate downregulated pathways associated with immune suppression, further highlighting LAPTM4B's role in modulating the tumor immune microenvironment.

Experimental knockdown of LAPTM4B in SK-MEL-48 cells (si-LAPTM4B) significantly reduced cell migration and invasion compared to si-control, as demonstrated by transwell assays (Figure 6H). Similarly, wound healing assays showed impaired wound closure in LAPTM4B-knockdown cells, further supporting its role in promoting cellular migration (Figure 6I). These findings confirm LAPTM4B's functional importance in driving tumor aggressiveness and its relevance as a key model-associated gene.

Discussion

Melanoma presents significant challenges due to its propensity for early metastasis and resistance to conventional therapies.[27] Despite advances in targeted and immunotherapies, survival rates for patients with advanced melanoma remain suboptimal.[28] This underlines the need for innovative approaches that not only refine prognostic predictions but also explore novel therapeutic avenues. In this study, we focus on triaptosis, a recently discovered form of programmed cell death (PCD), and its potential to uncover novel insights into melanoma progression, immune evasion, and therapeutic resistance.

Triaptosis represents a new frontier in the study of PCD, offering a promising target for cancer therapy.[18] While apoptosis and ferroptosis have been extensively studied in melanoma, triaptosis remains largely unexplored in this context. Our study presents compelling evidence that triaptosis-related activity plays a critical role in melanoma, with its associated signaling pathways showing significant variation across melanoma cell populations. Notably, epithelial cells, which dominate the melanoma tumor microenvironment, exhibited the highest triaptosis-related activity. This suggests

that triaptosis may be a key player in maintaining tumor survival and modulating immune responses within the tumor microenvironment.

The integration of single-cell RNA sequencing with bulk RNA-sequencing data enabled us to construct a robust prognostic model based on triaptosis-related signatures. Using a combination of machine learning algorithms, we identified a signature (TAS) that successfully predicted patient outcomes across multiple melanoma cohorts. The use of the SurvivalSVM model, which outperformed other algorithms in terms of concordance index (C-index), highlighted the robustness of the triaptosis-based approach. Our findings suggest that the TAS model not only has strong predictive power but also provides a deeper understanding of the molecular landscape of melanoma, especially regarding its immune microenvironment and triaptosis-related mechanisms.

One of the most striking aspects of this study is the identification of the tumor microenvironment (TME) as a key modulator of triaptosis activity. Our analysis revealed that the high-risk group, as determined by the TAS model, was characterized by increased immune and stromal scores, suggesting that triaptosis-related processes could influence the recruitment and function of immune cells within the TME. This observation is consistent with emerging research indicating that PCD pathways can alter the immune landscape of tumors, either by enhancing immune evasion or by promoting an immunosuppressive environment. In this respect, triaptosis could represent an important axis of immune modulation in melanoma, potentially influencing the effectiveness of current immunotherapies.

In addition to immune infiltration, we observed that the high-risk group also exhibited increased activation of several key signaling pathways, including those related to cell migration, invasion, and resistance to apoptosis. These findings suggest that triaptosis may be closely linked to processes that support melanoma metastasis and therapeutic resistance. Furthermore, pathway analysis revealed a significant association between the TAS model and several cancer-related pathways, underscoring the potential of triaptosis as a central player in melanoma pathogenesis.

Comparing our model to existing melanoma prognostic models revealed that the TAS model provides a distinct advantage in terms of its ability to predict patient outcomes across diverse datasets. While several established models have demonstrated predictive value, the incorporation of triaptosis-related features offers a more nuanced view of melanoma's molecular underpinnings, especially in relation to the TME and immune regulation. This could have important clinical implications, such as guiding patient stratification and informing personalized therapeutic decision-making. Patients identified as high-risk by the TAS model may benefit from intensified monitoring or combinatorial therapies targeting triaptosis-related pathways. Conversely, low-risk patients might be spared overtreatment, enabling more rational use of therapeutic resources.

In the future, the TAS model could serve as a valuable tool in clinical settings to optimize treatment strategies, particularly in the selection of immunotherapeutic or targeted approaches tailored to triaptosis activity levels. The integration of triaptosis-related biomarkers with existing clinical and molecular data could enhance the precision of melanoma management.

Importantly, the integration of machine learning algorithms with multi-omics data in this study provides a robust framework for melanoma prognosis that can be adapted to other cancers. The use of machine learning models, such as SurvivalSVM, to identify critical prognostic genes and pathways represents a powerful approach to improving clinical decision-making in melanoma. By enabling the accurate stratification of patients into high-risk and low-risk groups, this model can guide more precise therapeutic interventions, helping to identify patients who may benefit from novel treatment strategies targeting triaptosis-related pathways.

However, while our findings are promising, several questions remain to be addressed in future studies. The precise molecular mechanisms underlying triaptosis in melanoma, particularly how it interacts with other forms of PCD and the immune microenvironment, warrant further investigation. Moreover, the therapeutic potential of targeting triaptosis in melanoma remains to be fully explored. Future research should aim to validate the role of triaptosis-related genes and signaling pathways in preclinical and clinical settings, exploring the potential for novel drug development targeting this PCD pathway. Additionally, expanding the scope of this study to include other tumor types may provide insights into whether triaptosis is a universally relevant mechanism or a melanoma-specific phenomenon.

Conclusion

In summary, this study uncovers the critical role of triaptosis in melanoma progression and immune modulation, and introduces a novel triaptosis-based prognostic model (TAS) with strong predictive performance across independent cohorts. By integrating single-cell and bulk transcriptomic data with machine learning, the TAS model not only advances our understanding of melanoma biology but also demonstrates potential clinical utility for patient stratification and therapeutic guidance. Future research should focus on mechanistic validation and translational exploration of triaptosis-targeted interventions, which may pave the way for precision oncology approaches in melanoma and beyond.

Data Sharing Statement

All data needed to evaluate the conclusions in the paper are present in the paper and/or the Supplementary Materials. Additional data related to this paper may be requested from the authors.

Ethics Statement

This study was performed in accordance with the Declaration of Helsinki. Human primary cell lines included in this study were approved as part of this study protocol. This study was approved by Ethics Committee of the Xiangya Hospitai of Central South University.

Author Contributions

All authors made a significant contribution to the work reported, whether that is in the conception, study design, execution, acquisition of data, analysis and interpretation, or in all these areas; took part in drafting, revising or critically reviewing the article; gave final approval of the version to be published; have agreed on the journal to which the article has been submitted; and agree to be accountable for all aspects of the work.

Funding

The work was funded by grants from National Natural Science Foundation of China (grant number: 82073019).

Disclosure

The authors declare no competing interests.

References

1. Arnold M, Singh D, Laversanne M, et al. Global burden of cutaneous melanoma in 2020 and projections to 2040. *JAMA Dermatol*. 2022;158(5):495–503. doi:10.1001/jamadermatol.2022.0160
2. Leonardi GC, Falzone L, Salemi R, et al. Cutaneous melanoma: from pathogenesis to therapy (Review). *Int J Oncol*. 2018;52(4):1071–1080. doi:10.3892/ijo.2018.4287
3. Belote RL, Le D, Maynard A, et al. Human melanocyte development and melanoma dedifferentiation at single-cell resolution. *Nat Cell Biol*. 2021;23(9):1035–1047. doi:10.1038/s41556-021-00740-8
4. Dhanyamraju PK, Schell TD, Amin S, Robertson GP. Drug-tolerant persister cells in cancer therapy resistance. *Cancer Res*. 2022;82(14):2503–2514. doi:10.1158/0008-5472.CAN-21-3844
5. Swetter SM, Tsao H, Bichakjian CK, et al. Guidelines of care for the management of primary cutaneous melanoma. *J Am Acad Dermatol*. 2019;80(1):208–250. doi:10.1016/j.jaad.2018.08.055
6. Dyba T, Randi G, Bray F, et al. The European cancer burden in 2020: incidence and mortality estimates for 40 countries and 25 major cancers. *Eur J Cancer*. 2021;157:308–347. doi:10.1016/j.ejca.2021.07.039
7. Lopes FCPS, Sleiman MG, Sebastian K, Bogucka R, Jacobs EA, Adamson AS. UV exposure and the risk of cutaneous melanoma in skin of color: a systematic review. *JAMA Dermatol*. 2021;157(2):213–219. doi:10.1001/jamadermatol.2020.4616
8. Brunsgaard EK, Jensen J, Grossman D. Melanoma in skin of color: Part II. Racial disparities, role of UV, and interventions for earlier detection. *J Am Acad Dermatol*. 2023;89(3):459–468. doi:10.1016/j.jaad.2022.04.057
9. Saginala K, Barsouk A, Aluru JS, Rawla P, Barsouk A. Epidemiology of melanoma. *Med Sci*. 2021;9(4):63. doi:10.3390/medsci9040063
10. Caraban BM, Aschie M, Deacu M, et al. A narrative review of current knowledge on cutaneous melanoma. *Clin Pract*. 2024;14(1):214–241. doi:10.3390/clinpract14010018
11. Long GV, Swetter SM, Menzies AM, Gershenwald JE, Scolyer RA. Cutaneous melanoma [published correction appears in Lancet. 2023;402(10400):450. doi: 10.1016/S0140-6736(23)01581-7]. *Lancet*. 2023;402(10400):485–502. doi:10.1016/S0140-6736(23)00821-8
12. Tasdogan A, Faubert B, Ramesh V, et al. Metabolic heterogeneity confers differences in melanoma metastatic potential. *Nature*. 2020;577(7788):115–120. doi:10.1038/s41586-019-1847-2

13. El-Hachem N, Leclercq M, Susaeta Ruiz M, et al. Valine aminoacyl-tRNA synthetase promotes therapy resistance in melanoma. *Nat Cell Biol*. 2024;26(7):1154–1164. doi:10.1038/s41556-024-01439-2
14. Zou Y, Yaguchi T. Programmed cell death-1 blockade therapy in melanoma: resistance mechanisms and combination strategies. *Exp Dermatol*. 2023;32(3):264–275. doi:10.1111/exd.14750
15. Hsu SK, Li CY, Lin IL, et al. Inflammation-related pyroptosis, a novel programmed cell death pathway, and its crosstalk with immune therapy in cancer treatment. *Theranostics*. 2021;11(18):8813–8835. doi:10.7150/thno.62521
16. Berthenet K, Castillo Ferrer C, Fanfone D, et al. Failed apoptosis enhances melanoma cancer cell aggressiveness. *Cell Rep*. 2020;31(10):107731. doi:10.1016/j.celrep.2020.107731
17. Khorsandi K, Esfahani H, Ghamsari SK, Lakhshehei P. Targeting ferroptosis in melanoma: cancer therapeutics. *Cell Commun Signal*. 2023;21(1):337. doi:10.1186/s12964-023-01296-w
18. Swamynathan MM, Kuang S, Watrud KE, et al. Dietary pro-oxidant therapy by a vitamin K precursor targets PI 3-kinase VPS34 function. *Science*. 2024;386(6720):eadk9167. doi:10.1126/science.adk9167
19. Zhang C, Shen H, Yang T, et al. A single-cell analysis reveals tumor heterogeneity and immune environment of acral melanoma. *Nat Commun*. 2022;13(1):7250. PMID: 36433984. doi:10.1038/s41467-022-34877-3
20. Bogunovic D, O'Neill DW, Belitskaya-Levy I, et al. Immune profile and mitotic index of metastatic melanoma lesions enhance clinical staging in predicting patient survival. *Proc Natl Acad Sci U S A*. 2009;106(48):20429–20434. PMID: 19915147. doi:10.1073/pnas.0905139106
21. Jönsson G, Busch C, Knappskog S, et al. Gene expression profiling-based identification of molecular subtypes in stage IV melanomas with different clinical outcome. *Clin Cancer Res*. 2010;16(13):3356–3367. PMID: 20460471. doi:10.1158/1078-0432.CCR-09-2509
22. Mann GJ, Pupo GM, Campain AE, et al. BRAF mutation, NRAS mutation, and the absence of an immune-related expressed gene profile predict poor outcome in patients with stage III melanoma. *J Invest Dermatol*. 2013;133(2):509–517. PMID: 22931913. doi:10.1038/jid.2012.283
23. Jayawardana K, Schramm SJ, Haydu L, et al. Determination of prognosis in metastatic melanoma through integration of clinico-pathologic, mutation, mRNA, microRNA, and protein information. *Int J Cancer*. 2015;136(4):863–874. PMID: 24975271. doi:10.1002/ijc.29047
24. Budden T, Davey RJ, Vilain RE, et al. Repair of UVB-induced DNA damage is reduced in melanoma due to low XPC and global genome repair. *Oncotarget*. 2016;7(38):60940–60953. PMID: 27487145. doi:10.18632/oncotarget.10902
25. Cabrita R, Lauss M, Sanna A, et al. Tertiary lymphoid structures improve immunotherapy and survival in melanoma. *Nature*. 2020;577(7791):561–565. PMID: 31942071. doi:10.1038/s41586-019-1914-8
26. Xie J, Wu D, Zhang P, Zhao S, Qi M. Deciphering cutaneous melanoma prognosis through LDL metabolism: single-cell transcriptomics analysis via 101 machine learning algorithms. *Exp Dermatol*. 2024;33(4):e15070. doi:10.1111/exd.15070
27. Abbas O, Miller DD, Bhawan J. Cutaneous malignant melanoma: update on diagnostic and prognostic biomarkers. *Am J Dermatopathol*. 2014;36(5):363–379. doi:10.1097/DAD.0b013e31828a2ec5
28. Pollack LA, Li J, Berkowitz Z, et al. Melanoma survival in the United States, 1992 to 2005. *J Am Acad Dermatol*. 2011;65(5 Suppl 1):S78–S86. doi:10.1016/j.jaad.2011.05.030